Theoretical Studies of the Properties and Solution Chemistry of AnO_2^{2+} and AnO_2^{+} Aquo Complexes for An = U, Np, and Pu

P. Jeffrey Hay,* Richard L. Martin, and Georg Schreckenbach

Theoretical Division, Los Alamos National Laboratory, Los Alamos, New Mexico 87545

Received: February 9, 2000; In Final Form: April 20, 2000

The structures and vibrational frequencies of $UO_2(H_2O)_5^{2+}$, $NpO_2(H_2O)_5^{2+}$, and $PuO_2(H_2O)_5^{2+}$ corresponding to An(VI) oxidation states and $UO_2(H_2O)_5^{+}$, $Np(H_2O)_5^{+}$, and $Pu(H_2O)_5^{+}$ corresponding to An(V) have been calculated using density functional theory (DFT) and relativistic effective core potentials (RECPs). The resulting structures are compared to EXAFS solution studies, and the Raman and IR vibrational frequencies of the actinyl unit are compared to experimental studies in solution. Free energies for reactions in solution are computed by combining thermodynamic free energies in the gas phase with a dielectric continuum model to treat solvent effects. The hydrolysis reaction of $UO_2(H_2O)_5^{2+}$ to form $UO_2(H_2O)_4(OH)^{+}$ and the reactions for removing or adding a water to the first shell in $UO_2(H_2O)_5^{2+}$ are examined using this approach. Multiplet and spin−orbit effects not included in a single-configuration DFT wave function are incorporated by model spin−orbit CI calculations. PuO_2^{q+} is used as a model for the aquo complexes in a weak ligand field for the cases $q = 3$ ($5f^1$ configuration), $q = 2$ ($5f^2$) and $q = 1$ ($5f^3$). The inclusion of these effects results in a different ground state for $NpO_2(H_2O)_5^{2+}$ and $PuO_2(H_2O)_5^{2+}$ than that obtained in the original DFT calculations. The reduction potentials for all three $AnO_2(H_2O)_5^{2+}$ complexes in solution is compared with electrochemical experimental data. The trend for the reduction potentials $NpO_2(H_2O)_5^{2+} > PuO_2(H_2O)_5^{2+} > UO_2(H_2O)_5^{2+}$ is found in agreement with experiment, when multiplet and spin−orbit corrections are included, although the absolute reduction potentials are overestimated in all three cases. The possible reasons for this overestimate are examined using all-electron calculations using the ADF method.

I. Introduction

The chemistry of actinide species in solution is characterized by a variety of oxidation states and coordination numbers about the actinide center as well as monomeric, dimeric, and polymeric species.[1,2] For these reasons and their inherent radioactive nature, obtaining reliable properties of actinide species remains a challenge for the experimentalist. Similarly actinide species present numerous difficulties for theoretical studies[3] by virtue of the importance of relativistic effects, the large number of low-lying electronic states for $5f^n$ configurations, and the comparable magnitude of spin−orbit, multiplet, and correlation effects.

Recently density functional theory (DFT)[4] has begun to be applied to actinide species with very promising results concerning the structures and vibrational properties.[5] Recently we have applied DFT techniques to study the properties of the hexafluorides[6] and actinyl hydroxide complexes[7,5] In this paper we apply "hybrid" density functional approaches to the actinyl aquo complexes, which are among the most prevalent families of actinide complexes in aqueous solution at low pH. In particular we examine $AnO_2(H_2O)_5^{2+}$ and $AnO_2(H_2O)_5^{+}$ corresponding to the +6 and +5 oxidation states, respectively, of the actinides An = U, Np, and Pu. These were chosen since there are solution EXAFS[8−13] and X-ray measurements[14] are available for many of these species. In addition the vibrational frequencies are computed at the equilibrium structures using analytic second derivatives. A systematic analysis of the Raman and infrared actinyl stretching frequencies is compared with available experimental measurements.[12,15−19]

Actinyl complexes have become the focus of increasing attention by theoretical calculations using a variety of techniques. Hydrated forms of the actinyl have been studied using DFT[11,20] approaches, and Hartree−Fock-based approaches, have been used to study hydrates[21] and as well as nitrate and sulfate complexes.[22] Extensive studies of the low-lying states of the "bare" triatomic AnO_2^{q+} species have been made[23−27] to compare with matrix spectroscopic data.

II. Details of the Calculations

In most of the calculations presented here the electronic structure of the actinyl complexes is treated using the B3LYP hybrid density functional[28,29] approach. Relativistic effective core potentials[6] are used on U, Np, and Pu to replace the inner 78 electrons. The 6s and 6p outer core electrons, as well as the valence 5f, 6d, 7s, and 7p electrons, are explicitly treated using a [3s 3p 2d 2f] contracted Gaussian basis. The 6-31G* basis is used to treat the C, O, and H atoms in the calculations.

All geometries are fully optimized at the B3LYP level and vibrational frequencies are calculated using analytic second derivatives. All structures are verified to be actual minima with all real frequencies. In cases where imaginary frequencies are found, the structures are reoptimized until actual minima are found.

For comparison purposes we also present selective results using Hartree−Fock as well as local density (SVWN)[30] and gradient-corrected (BLYP)[31,29] density functional approaches. All calculations were carried out using the Gaussian98 program.[32]

Solvent calculations were carried out using the BSJ dielectric continuum model.[33] The molecule is surrounded by a cavity

* Corresponding author. E-mail: pjhay@lanl.gov.

10.1021/jp000519h CCC: $19.00
Published on Web 06/14/2000

constructed from spheres about each atom. The following atomic radii (Å) are used in these calculations: O (1.576), H(1.172), U, Np, and Pu (2.05). The solvent response is determined by solution of Poisson's equation on the boundary surface with a dielectric constant (ϵ) of 1 inside the cavity and 78.1 for water outside the cavity. From the induced charges on the surface one obtains the free energy of solution of the molecule. The atomic radius for U was chosen to be similar to the value used for Fe in an earlier study of hydrolysis chemistry.[34] The calculated free energy of the uranyl hydrolysis reaction (vida infra) was computed starting with this radius and varying the radius by about 10% in either direction. The calculated reaction free energy was fairly invariant to these changes and varied by only a few kcal/mol over this range.

Effects of multiplet splitting and spin−orbit interactions not present in the DFT single configuration ground state were probed by configuration interaction calculations on PuO_2^{+q} species. A Hartree−Fock SCF calculation on the PuO_2^{2+} ($5f\delta^2$) ground state with $R_{Pu-O} = 1.75$ Å was used to define the 5fδ orbitals. The 5fϕ and 5fπ excited orbitals were determined using the improved virtual orbital method and a cylindrically averaged PuO_2^{3+} ion state. The order of these orbital energies are not too different from the order of virtual orbitals in $UO_2(H_2O)_5^{2+}$ from the DFT calculations For the states of PuO_2^{2+} and PuO_2^{1+}, all configurations arising from two and three electrons, respectively, in these six orbitals were generated. These calculations were carried out using the MESA code.[35]

In addition to these multiplet effects, the influence of spin−orbit coupling must also be considered. The CI results of PuO_2^{q+}, were used as a starting point to form spin−orbit coupling matrix elements construct using an approximate method employing an effective one-electron spin−orbit operator

$$V_{so} = \zeta\,[l_z s_z + {}^1/_2\, l_+ s_- + {}^1/_2\, l_- s_+] \qquad (1)$$

where the spin−orbit coupling constant is taken from atomic calculations. The coupling constants for the 5f orbital of U^{3+}, Np^{3+}, and Pu^{3+} were taken as 1906, 2190, and 2484 cm^{-1}, respectively. In these model calculations each matrix element between $\Phi_J(\Lambda,S)$ states

$$\langle I|V_{so}|I\rangle = \langle \Phi_I(\Lambda,S)|V_{so}|\Phi_I(\Lambda,S)\rangle + E_I^{CI} \qquad (2)$$

$$\langle I|V_{so}|J\rangle = \langle \Phi_I(\Lambda,S)|V_{so}|\Phi_J(\Lambda,S)\rangle \qquad (3)$$

was evaluated assuming a single-configuration representation in terms of complex orbitals with the appropriate Λ quantum number for the spin−orbit interactions. The energies of the CI roots without spin−orbit coupling were used as the energy terms E_I^{CI} in the diagonal elements.

Comparison of calculated ionization potentials were made between the results of using LDA and BLYP functionals with RECPs using Gaussian 98 and the results of all-electron frozen core results with the same functionals using the ADF code.[36,37] ADF single point calculations were performed at the Gaussian98-ECP optimized geometries as follows. LDA calculations used the LDA-ECP optimized geometry of $[UO_2(H_2O)_5]^{2+}$, whereas BLYP (GGA) calculations used the BLYP-ECP optimized geometry for the same molecule. The same geometry was employed for both the U(VI) and the U(V) molecule in each case. Scalar relativistic effects are accounted for by means of the quasi-relativistic (Pauli) method; spin−orbit effects are neglected. The standard ADF basis sets IV (U) and V (O, H) were used. These are Slater type basis sets of triple-ζ quality in the valence region. They contain one (U) or two (O, H) sets of polarization functions, respectively. All shells up to and including the 5d (U) and 1s (O) shells, respectively, were considered as core and kept frozen in molecular calculations. The valence orbitals are orthogonalized to all core orbitals in the molecule.

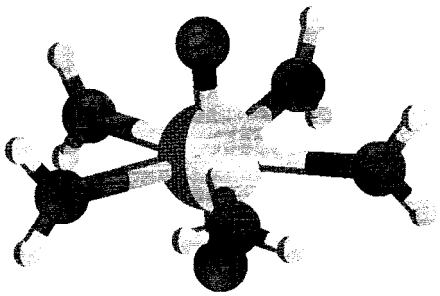

Figure 1. Calculated structure of $UO_2(H_2O)_5^{2+}$ from B3LYP calculations.

III. Results and Discussion

In the following section (III.A) we present the structures and vibrational frequencies of actinyl aaquo complexes using DFT approaches, and the results are compared to available experimental EXAFS structural and Raman spectroscopic studies in solution. In the next section (III.B) we explore two reactions of $UO_2(H_2O)_5^{2+}$ in solution where the results of DFT calculations are combined with a dielectric continuum model to incorporate the effects of the solvent. We then examine (III.C) the effects of multiplet and spin−orbit interactions for actinyl aquo species with unpaired 5f electrons. These interactions can affect the nature of the electronic ground state, and they can also affect relative energies when comparing molecular species with different numbers of 5f electrons. While such effects would not affect the results of the first two sections, they can be important in redox processes, which are discussed in the final section (III.D). In this section the reduction potentials of $UO_2(H_2O)_5^{2+}$ and the Np(VI) and Pu(VI) counterparts are treated systematically combining DFT results with calculated corrections for multiplet and spin−orbit effects.

A. Properties of Actinyl Complexes. The predominant form of the +5 and +6 oxidation states of the actinides at low pH are the penta-aqua species $AnO_2(H_2O)_5^{+}$ and $AnO_2(H_2O)_5^{2+}$, respectively. In this section the calculated structures for the actinide series U, Np, and Pu for both oxidation states are presented from the results of density functional calculations. In all cases the geometries have been obtained without any symmetry constraints and the vibrational frequencies have been calculated at the resultant optimized structure. All structures presented, unless otherwise noted, correspond to minima with no imaginary frequencies.

Effects of Density Functionals. We first consider the closed-shell $UO_2(H_2O)_5^{2+}$ species. As is the case with the other molecules in this series, $UO_2(H_2O)_5^{2+}$ adopts the structure with an essentially linear O═U═O group and the coordinating water molecules bound in the equatorial plane of the uranyl group (See Figure 1). Calculations were carried out at the Hartree−Fock level and with density functional theory using local density (SVWN), gradient-corrected (BLYP), and hybrid (B3LYP) functionals. The optimum geometries were determined for each of these four methods and the vibrational frequencies were

TABLE 1: Comparison of Predictions of Structural and Vibrational Properties of $UO_2(H_2O)_5^{2+}$ Using Various Levels of Theory

	R(An = O) (Å)	R(An-O_{eq}) (Å)	ν_s (cm^{-1})	ν_{as} (cm^{-1})
HF, present	1.694	2.545	1091	1149
LDA (SVWN), present	1.778	2.423	854	945
BLYP, present	1.803	2.516	787	893
B3LYP, present	1.756	2.516	910	1003
BLYP[20]	1.746	2.550		
DK-AIMP[11]	1.750	2.421		
experimental				
EXAFS, soln[9]	1.76	2.41		
XRD, soln[14]	1.70	2.42		
XRD, solid[61]	1.71 ± 0.08	2.45 ± 0.10		
Raman, IR[16,19]			869	965

calculated at the respective minima. In Table 1 we compare the calculated U═O and U−OH_2 bond lengths as well as the symmetric and asymmetric vibrational modes of the uranyl group. The results are compared with available experimental data in solution using EXAFS measurements.

The Hartree−Fock results underestimate the U═O bond length by 0.07 Å and overestimate the equatorial U−O bond length by 0.13 Å. For the axial U═O bond length, the local density and hybrid functionals agree within 0.02 Å with experiment while the gradient corrected result is 0.04 Å longer than the EXAFS results. For the equatorial bonds the local density result is very close to experiment while the other methods overestimate the bond length by 0.10 Å or more. Since the motion of water molecules in the equatorial bonds corresponds to a softer vibrational frequency, it is not surprising that there is a wider variation in the bond lengths. The vibrational frequencies track the bond lengths in that higher frequencies are calculated when the bonds are shorter, as in Hartree−Fock, and vice versa when the bonds are longer. The SVWN and B3LYP give Raman frequencies 20 cm^{-1} below and 40 cm^{-1} above, respectively, the observed band at 869 cm^{-1}. Similar behavior is also noted for the infrared active actinyl asymmetric stretch observed at 965 cm^{-1}. While the local density and hybrid B3LYP are rather comparable for structural properties, we shall be presenting results of the hybrid B3LYP functional in the remainder of the paper since local density calculations typically overestimate properties relating to relative energies such as binding energies.

General Electronic Structure Considerations for Actinyls. The U(VI) species corresponds formally to a $5f^0$ state with no unpaired electrons on the metal and the oxygen atoms as formal −2 anions. While one would expect that the more weakly bound equatorial water molecules would modify the electronic structure of the uranyl, the vibriations in the electronic structure as a function of metal and oxidation state can be obtained by considering just the actinyl unit. The highest occupied levels in the "bare" actinyl species arise from sigma (σ_g and σ_u) and pi (π_g and π_u) molecular orbitals originating primarily in the O orbitals involved in the O═U═O bond. In particular, the σ_u orbital has a significant admixture of $5fz^3$ ($5f\sigma_u$). Also the π_u orbital has a small component of $5f\pi$. As shown schematically in Figure 2, the lowest unoccupied levels, of which there are two sets of degenerate orbitals in the absence of spin−orbit coupling, arise from the $5f\delta$ and $5f\phi$ orbitals. As a result, the overall ordering $5f\delta < 5f\phi < 5f\pi \ll 5f\sigma$ are the results for the lowest virtual orbitals in the actinyl species because of the participation of the $5f\pi$ and $5f\sigma$ orbitals in the occupied MOs of the actinyl. In these calculations and in other results in the literature on "bare" actinyls and actinyl complexes, the $5f\delta$ orbital is indeed found to be slightly lower in energy with a small separation between it and the $5f\phi$ orbital. As one goes down the $AnO_2L_5^{2+}$ series for An = U, Np and Pu then one would expect one unpaired electron ($S = 1/2$) for Np with $(5f\delta)^1$ configuration and two unpaired electrons ($S = 1$) for Pu with a $(5f\delta)^2$ configuration, as shown in Figure 2. The orbitals containing the unpaired electrons are nonbonding with respect to the actinyl unit, since there are no filled orbitals with these symmetries.

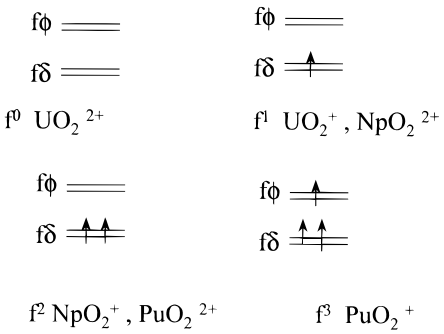

Figure 2. Schematic MO representation for ground states of the $AnO_2(H_2O)_5^{q+}$ species assuming occupation of the orbitals with lowest energies.

TABLE 2: Comparison of Calculated (B3LYP) and Experimental Properties of Actinyl Aqua complexes for both the An(VI) and An(V) Oxidation States

	$UO_2(H_2O)_5^{2+}$		$NpO_2(H_2O)_5^{2+}$		$PuO_2(H_2O)_5^{2+}$	
	calcd	exptl	calcd	exptl	calcd	exptl
R(An═O), Å	1.756	1.76,[a] 1.78[b]	1.752	1.75[h,i]	1.742	1.74[k]
R(An-O_{eq}), Å	2.516	2.41,[a] 2.41[b]	2.50	2.42[h,i]	2.485	2.41[k]
ν_s, cm^{-1}	908	870[c] 869[d]	854	854[g] 863[c]	805	833[g] 835[c]
ν_{as}, cm^{-1}	1001	965[e] 962[i]	983	969[e]	951	962[e]

	$UO_2(H_2O)_5^{+}$		$NpO_2(H_2O)_5^{+}$		$PuO_2(H_2O)_5^{+}$	
	calcd	exptl	calcd	exptl	calcd	exptl
R(An═O), Å	1.810		1.81	1.83[a] 1.83[j]	1.808	1.81[k]
R(An-O_{eq}), Å	2.616		2.61	2.50[a] 2.52[j]	2.61	2.47[k]
ν_s, cm^{-1}	840		794	767[c] 767[i]	718	748[g]
ν_{as}, cm^{-1}	909		904	824[e]	871	

[a] Allen et al. (1997), ref 9. [b] Wahlgren et al. (1999), ref 11. [c] Basile et al. (1974), ref 15. [d] Toth and Begun (1981), ref 16. [e] Jones and Penneman (1953), ref 19. [f] Guillaume et al. (1982), ref 18. [g] Madic et al. (1984), ref 17. [h] Clark et al. (1999), ref 13. [i] Tait et al. (1999) ref 12. [j] Combes et al. (1992), ref 8. [k] Conradson (1998), ref 10.

Structures and Vibrational Frequencies. For the series of complexes $AnO_2(H_2O)_5^{2+}$, one sees a very slight contraction in the actinyl bond from 1.76 Å for U (1.76 Å, exptl) to 1.742 Å for Pu (1.74 Å, exptl) as one progresses along the series U to Pu (Table 2). While the actinyl bond lengths are accurately predicted at the B3LYP level, the average U-equatorial O bond lengths are overestimated by ~0.1 Å. The predicted bond lengths to the equatorial ligands decrease by 0.03 Å in going from U(VI) to Pu(VI).

For the series $AnO_2(H_2O)_5^{+}$ corresponding to the An(V) oxidation state, the calculated values of the actinyl bond lengths are all calculated to be about 1.81 Å, or 0.05 Å longer than the An(VI) analogues, as shown in Table 2. Similarly little variation with metal is seen for the calculated actinide−water bond lengths, all about 2.62 and 0.1 A longer than the corresponding An(VI) species. The electronic structure for these molecules at

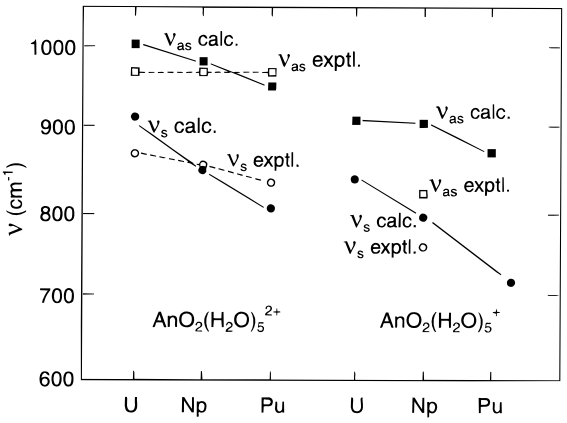

Figure 3. Calculated and experimental frequencies for the actinyl symmetric and asymmetric stretch modes in $AnO_2(H_2O)_5^{2+}$ and $AnO_2(H_2O)_5^{+}$ species.

TABLE 3: Atomic Populations and Overlap Populations in the $AnO_2(H_2O)_5^{2+}$ Series from Mulliken Population Analyses

atomic populations	U	Np	Pu
s	2.214	2.227	2.221
pσ	1.841	1.822	1.795
pπ	4.315	4.225	4.228
p tot	6.157	6.046	6.024
dσ	0.398	0.386	0.365
dπ	0.680	0.646	0.620
dδ	0.183	0.267	0.263
d tot	1.261	1.299	1.248
fσ	1.366	1.394	1.438
fπ	1.162	1.196	1.247
fδ	0.030	1.028	1.988
fϕ	0.152	0.189	0.212
f tot	2.710	3.807	4.885
q tot	1.658	1.621	1.622
overlap population	0.362	0.349	0.330

the DFT level correspond to $S = {}^1/_2$ (δ^1) for U(V), $S = 1$ (δ^2) for Np(V), and $S = {}^3/_2$ ($\delta^2\,\phi^1$) for Pu(V) where high spin coupling is maintained in all cases among the low-lying 5f electrons (see Figure 2).

For the vibrational frequencies we focus first on the symmetric (Raman active) and asymmetric (infrared active) stretching modes of the actinyl group. As seen in Table 2 and Figure 3, the symmetric mode lies at lower energy and decreases from 908 cm^{-1} (exptl, 872 cm^{-1}) to 805 cm^{-1} (exptl, 836 cm^{-1}) across the series $UO_2(H_2O)_5^{2+}$ to $PuO_2(H_2O)_5^{2+}$. The infrared active asymmetric stretch modes are predicted to lie at 1001, 983, and 951 cm^{-1} for U, Np, and Pu, respectively, while the experimental results of Jones and Penneman[19] nearly 50 years ago observe this mode to lie near 965 cm^{-1} in all three complexes. For the $An(H_2O)_5^{+}$ series we find the symmetric mode to lie 60−70 cm^{-1} lower in energy and the asymmetric mode to lie 80−90 cm^{-1} lower in energy than the $An(H_2O)_5^{2+}$ counterpart.

An interesting question concerns why the vibrational frequencies of the actinyl bond are decreasing going down the series while the bond length is getting shorter, since that would normally imply a stronger bond. To analyze this point further, we examined the atomic populations and overlap populations in the An(VI) series (Table 3). For the U(VI) species, formally a f^0 (and d^0) configuration, the net f and d populations are 2.71 and 1.26, respectively, indicating considerable participation of these orbitals compared to the ideal ionic case. In particular, one sees strong participation of the f_σ orbital in the actinyl bond. However, one does not observe any variation of these populations in going to Np and Pu except for the increase in the fδ orbitals as the number of unpaired electrons increases. No apparent trend is evident in the s and p orbital participation. However, the net overlap population steadily decreases by about 10% across this series, which we attribute to the smaller size of the 5f orbitals as atomic number increases. Given essentially constant *f* and d orbital participation across the series, the decrease in stretching frequency appears to correlate with the decreased overlap with the 5f orbital.

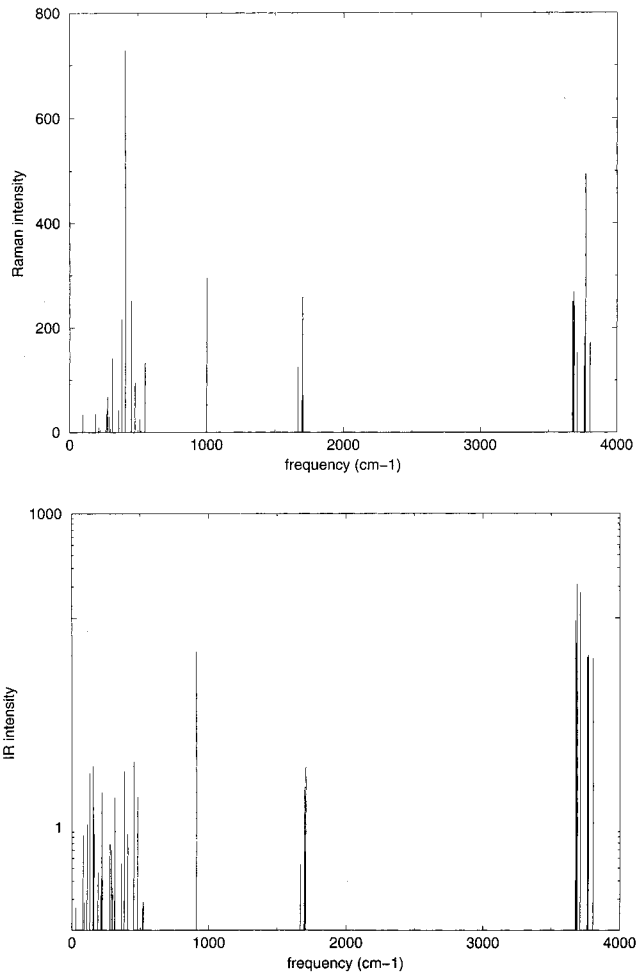

Figure 4. Calculated Raman (upper part) and vibrational (lower part) intensities for the normal modes of $UO_2(H_2O)_5^{2+}$.

TABLE 4: Vibrational Modes of $UO_2(H_2O)_5^{2+}$

description of mode	calculated frequencies (cm^{-1})
H_2O librational modes	22, 31, 81, 90, 97, 111, 130, 155, 157, 161
O═U═O bend	213, 222
U−OH_2 stretch	261, 273, 297, 311,313
U−H_2O twisting	191, 218, 278, 288, 361
H_2O wag	383, 408, 451, 479
H_2O tilt	503, 514, 522, 547, 554
O═U═O sym stretch	908
O═U═O asym stretch	1001
H−O−H bend	1669, 1696, 1698, 1701, 1707
H−O−H stretch (sym)	3675, 3677, 3682, 3688, 3709
H−O−H stretch (asym)	3762, 3763, 3768, 3770, 3804

In Table 4, the calculated frequencies are given for $UO_2(H_2O)_5^{2+}$ aquo species along with their normal mode descriptions. In Figure 4 we display the calculated Raman and infrared vibrational intensities for the same molecule. In addition to the asymmetric and symmetric stretch modes discussed above, we note the two O═U═O bending modes near 270 cm^{-1}. At higher frequencies one finds the bending (∼1700 cm^{-1}) and stretching (∼3700 cm^{-1}) modes of the water molecule which have been

TABLE 5: Comparison of Various Optimized and Idealized Structures of $UO_2(H_2O)_5^{2+}$ from B3LYP Calculations

structure (symmetry)	total energy (au)	relative energy (kcal/mol)	no. of imaginary modes	H_2O orientation
no symmetry	−583.668 899	0.0	0	$R(U{=}O) = 1.756$ $R(U{-}OH_2) = 2.516$
D_5	−583.668 742	0.1	2	$R(U{=}O) = 1.756$ $R(U{-}OH_2) = 2.513$
D_{5h}	−583.667 738	0.6	3	$R(U{=}O) = 1.758$ $R(U{-}OH_2) = 2.513$

perturbed by the interactions with the actinyl and with the other water molecules.

The details of the structures of the aquo complexes with respect to the orientation of the water molecules are very sensitive to the density functional and level of basis set employed in the calculation. In most of the complexes the water molecules are nearly perpendicular to the equatorial plane, with the plane of the water canted slighly from vertical. All of the optimizations were carried out without any assumptions with regard to overall symmetry of the molecule, and the final structures typically have only C_1 point group symmetry. The optimal structures reported here have all real vibrational frequencies corresponding to actual minima. The computed structure for $UO_2(H_2O)_5^{2+}$ at the B3LYP level of DFT theory using a 6-31G* basis on the ligand and the valence double-ζ contracted basis on the U actually has four water molecules oriented nearly perpendicular (to the equatorial plane) and one nearly planar (in the equatorial plane), Figure 1. The calculated structure for $UO_2(H_2O)_5^{+}$ has all 5 water molecules nearly perpendicular with approximate D_5 symmetry.

To examine this issue further, optimizations were carried out for the two cases where symmetry was rigorously imposed (a) with all five water molecules canted in D_5 symmetry and (b) with all five water molecules exactly perpendicular with D_{5h} symmetry. The results are shown in Table 5, where it is seen that the D_5 structure lies only 0.1 kcal/mol higher than the actual optimized structure with no symmetry. The D_5 structure is found to have two imaginary frequencies. The D_{5h} structure, with three imaginary frequencies is calculated to lie 0.6 kcal/mol higher than the true minimum. In Table 1, where we compared other DFT results as well as HF results, one notes that the HF and LDA (SVWN) structures have approximate D_5 symmetry with all five water molecules canted, whereas the B3LYP structure has one molecule nearly planar.

The actinyl species of Np and Pu in Table 2 are all true minima for the basis set employed in the B3LYP calculations. They also show small differences between various orientations of the water molecules, but we will not attribute great importance to these conformational differences.

B. Solution Chemistry of Actinyls. The calculations up to this point have considered the actinyl and its first coordination shell of water molecules as gas phase species. To examine the chemistry of these species in solution it is necessary to incorporate the effects of the solvent in a consistent manner. This is particularly important in view of the highly charged nature of these species. For this purpose we adopt the dielectric continuum model[33] discussed in the Methods section to provide a relatively simple description of the response of the solvent to the electronic properties of the actinyl species. In this model the molecule is surrounded by a surface comprised of spheres about each atom and the solvent is represented by a continuum dielectric with dielectric constant ($\epsilon = 78.1$) outside the surface. The electronic distribution of the solute molecule is represented by effective charges fit to the electrostatic potential. From a solution of Poisson's equation, the free energy of solvation of the molecule is then determined. This quantity is added to the gas-phase free energy to obtain thermodynamic properties in solution.

Hydrolysis Reaction of $UO_2(H_2O)^{2+}$. The reaction of $AnO_2(H_2O)_5^{2+}$ species with water to form the hydroxide

$$UO_2(H_2O)_5^{+2} + H_2O \rightarrow UO_2(H_2O)_4(OH)^{+} + H_3O^{+} \quad (4)$$

is a typical reaction at low pH for U(VI), Np(VI), and Pu(VI) as well as for the An(V) oxidation states. We examine the hydrolysis reaction for the U(VI) species here following the same approach used earlier to study Fe(III) hydrolysis.[34] The calculated U=O bond lengths are 1.779 and 1.786 Å, respectively. The $UO_2(H_2O)_4(OH)^{+1}$ species has a linear U−O−H linkage with a U−OH bond length of 2.162 Å.

The thermodynamic properties of all species at 298 K were calculated as summarized in Table 6. The first entry E^0_{elec} represents the differences in electronic energies of the products and reactants above with zero-point corrections included. The next entry ΔG^{298} corresponds to the reaction energy when the vibrational and other thermodynamical contributions to the gas-phase free energies of each species have been added. The reaction free energy is predicted to be −29 kcal/mol in the gas-phase according to ΔG^{298}. To compute values in solution, the solvation free energies of both uranium species in eq 4 are calculated according to the BSJ method described above. In the case of the aqua complex, the five water molecules chemically bound to the uranyl are explicitly treated quantum mechanically while the water molecules in the next coordination shells are implicitly incorporated in the delectric cavity. Similarly the solvation energies of H_2O and H_3O^+ were computed with using the BSJ method using a dielectric cavity about each molecule. From these individual solvation energies, an overall free energy in solution for the reaction, ΔG^{soln}. is obtained. In solution the reaction is now *endothermic* by +17 kcal/mol in contrast to the gas phase energetics.

Experimentally the equilibrium constant for the U(VI) hydrolysis corresponds to an endoergic reaction of +4.3 kcal/mol.[38] The solvent corrections preferentially stabilize the doubly charged actinyl species relative to the singly charged ones, as expected from a simple Born cavity model where the stabilization is proportional to q^2. (In these studies a more realistic cavity resembling a van der Waals surface cavity is used in calculating the solvent effects.) Since the atomic radius and the dielectric constant are the only parameters needed for the solvation calculations, we investigated variations of the actinide atomic radius about the value of 2.05 Å, but this had little effect on the reaction free enegy. Overall there remains about a 13 kcal/mol energy difference between the experimental and theoretical values for the free energy of this reaction in solution. We repeated these calculations in a slightly larger basis set (uncontracted on U, 6-31+G* on O) and found the solution free energy to be +13 kcal/mol, in slightly better agreement with experiment. Our previous experience with Fe(III) hydrolysis[34] led to much smaller errors (a few kcal/mol) for reaction energies in solution compared with experiment. While the current results for actinides may be reflective of the overall absolute error in the combination of electronic structure and solvation models, calculations of this type should be able to predict relative energies in a series of molecules as features are systematically varied.

Removal and Addition of Water to the First Coordination Sphere of $UO_2(H_2O)_5^{2+}$. The focus of this paper has been on

TABLE 6: Calculated Reaction Energies (kcal/mol) for Actinyl Processes in Solution[a]

	E_{elec}	E^0_{elec}	ΔG^{298}	ΔG^{soln}	ΔG^{soln}(corr)	ΔG^{expt}
hydrolysis reaction						
$UO_2(H_2O)_5^{2+} + H_2O \rightarrow UO_2(H_2O)_4(OH)^{1+} + H_3O^+$		−22.4	−29.0	+13.2		+4.7[b]
ligand addition reactions						
B3LYP (present calculations)						
$UO_2(H_2O)_4^{2+} + H_2O \rightarrow UO_2(H_2O)_5^{2+}$	−28.9	−27.2	−19.3	−2.3	−6.5	
$UO_2(H_2O)_5^{2+} + H_2O \rightarrow UO_2(H_2O)_6^{2+}$	−22.4	−19.5	−9.7	+5.7	+1.5	
BLYP (ref 20)						
$UO_2(H_2O)_4^{2+} + H_2O \rightarrow UO_2(H_2O)_5^{2+}$	−23.4 (−7.2)[c]					
$UO_2(H_2O)_5^{2+} + H_2O \rightarrow UO_2(H_2O)_6^{2+}$	+4.0 (+18.5)[c]					

[a] Quantities refer to electronic energy E_{elec}, electronic + zero point E^0_{elec}, gas-phase free energy ΔG^{298}, solution free energy ΔG^{soln}, solution free energy (corrected for TS_{tr}) ΔG^{soln}(corr), and experimental solution free energy ΔG^{exptl}. [b] Ref. 38. [c] Including dielectric solvent effects.

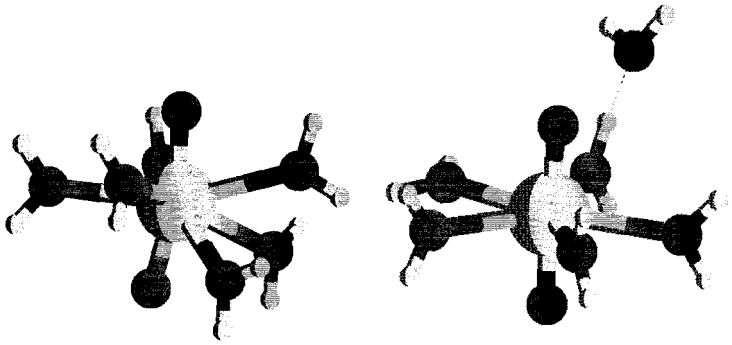

Figure 5. Calculated structure of two local minima for structures from B3LYP calculations, one with six waters in the first coordination sphere and one with five waters and one water in the first and second coordination spheres, respectively.

the pentaaquo complexes of the AnO_2^{2+} and AnO_2^{1+} species, since it is reasonably well established that the actinyl species are coordinated to five water molecules in solution from EXAFS[8−13] and NMR[39] studies. We note, however, that a recent EXAFS study[10] found the number of water molecules coordinated PuO_2^+ and PuO_2^{2+} in the aquo complexes to be 4 and 6, respectively. To investigate the relative energies involved in either adding a water molecule to the first coordination sphere to produce a six-coordinate species or removing one to produce a four-coordinate species, we carried out calculations on uranyl surrounded by four, five and six water molecules. For each structure the geometry was optimized, vibrational frequencies were computed, and the effects of solvent were calculated.

The optimized structure of $UO_2(H_2O)_4^{2+}$ was found to have D_{4h} symmetry from B3LYP calculations with all four water molecules oriented perpendicular to the equatorial plane. The calculated U═O and U−OH_2 bond lengths were 1.776 and 2.428 Å, respectively. For the $UO_2(H_2O)_6^{2+}$ complex, one structure was obtained (Figure 5) with six water molecules in the first coordination shell with a U═O bond length of 1.763 Å and U−OH_2 bond lengths ranging from 2.519 to 2.610 Å (for an average of 2.563 Å). This structure is a true minimum with all real vibrational frequencies. Another stable isomer was also found (Figure 5) with five water molecules in the first coordination shell and a sixth water hydrogen-bonded to one of the other water molecules. This structure was 3.8 kcal/mol lower in energy than the six-coordinate form.

The relative energies of uranyl species with 4, 5, and 6 water molecules in the first coordination sphere are summarized in Table 6. Comparing calculated gas phase free energies at 298 K, the five-coordinate species is more stable than water plus the four-coordinate species by 19 kcal/mol. The same comparison also shows the six-coordinate species to be more stable, but by only 10 kcal/mol, than the five-coordinate species plus water. Using only electronic energies plus zero-point corrections, i.e., without considering the thermal contributions at 298 K, the reaction energies for adding a fifth and sixth water would have been even more exothermic (27 and 20 kcal/mol, respectively).

When solvent effects are included, significant effects on the relative stabilities are observed. Addition of the fifth water molecule is still exothermic, but only by 2.3 kcal/mol. The formation of the six-coordinate species is now *endothermic* by 5.7 kcal/mol. These results are schematically shown in Figure 6. Since all species have the same +2 charge, there is no gross solvent stabilization due to difference in charges as we will see in subsequent sections. For a given ligand addition reaction, the molecule with fewer water molecules coordinated has a smaller effective volume which can be solvated more effectively than the larger counterpart. This would have the net effect of reducing the overall exothermicity of the gas phase reaction.

While the calculations thus successfully predict five-coordination as the preferred mode for UO_2^{2+} species in solution, there is one additional thermodynamic correction that needs to be included.[34] The ΔG^{298} gas-phase value for each reaction was computed with each species at 1 atm pressure. For the concentrations of water in aqueous solution, however, the effective pressure is 1354 atm. This contributes an overall decrease (−4.3 kcal/mol) in the free energy of the reaction, arising from the decrease in translational entropy of the water molecule, as shown in the ΔG_{corr} column of Table 6. This can be seen by noting that a decrease in entropy in the reactants in eq 6 for the overall reaction free energy,

$$\Delta G = H_{prod} - TS_{prod} - H_{react} + TS_{react} \qquad (5)$$

as the pressure is increased from 1 to 1354 atm, will decrease the free energy of the reaction. This translational entropy correction is discussed more fully in the context of absolute solvation energy of transition metal ions.[34] When all of the

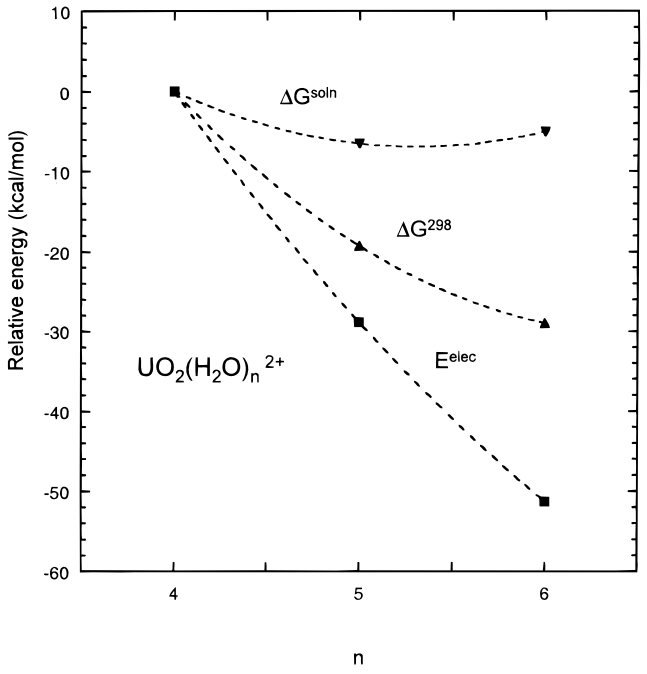

Figure 6. Relative energies of $UO_2(H_2O)_4^{2+}$ $UO_2(H_2O)_5^{2+}$ and $UO_2(H_2O)_6^{2+}$ from electronic energies, gas phase, and solution free energies.

solvation and thermodynamic effects have been included, five coordination is still predicted to be the most favorable structure. However, the difference compared to the six-coordinate structure is only 1.5 kcal/mol. The experimental studies of uranyl hydration in solution all point to five coordination as the most consistent structure with the EXAFS data.

The hydration of UO_2^{2+} was also recently examined by Spencer et al.[20] who employed the BLYP functional to determine the structures of uranyl surrounded 4, 5, and 6 water species. A high-symmetry geometry (D_{nh}) was assumed for each species with the water molecules oriented perpendicular to the equatorial plane, and no vibrational analysis was carried out. The relative stability of the *electronic energies* was examined, and the five-coordinate form was found to be most stable, whereas in our B3LYP studies we find the gas-phase electronic energies to favor the six-coordinate form. The relative energies of the five- and six-coordinate species in the gas phase are −22.4 kcal/mol in the present calculations compared to +4.0 kcal/mol reported by Spencer et al.[20] They also then added a continuum dielectric correction, but without any thermodynamic contributions to the electronic energy to obtain free energies. The relative ordering was preserved in their analysis with solvation effects, while we found that only when solvation effects were included was the five-coordinate species the most stable. We would also note that a recent study by Rempe et al.[40] on hydration of Li^+ also found the hydrates to have relative energies $Li(H_2O)_6^+ < Li(H_2O)_5^+ < Li(H_2O)_4^+$, but that this trend was reversed to favor four-coordination was obtained when thermodynamic and solvation effects were included.

C. Multiplet and Spin−Orbit Effects on Electronic Structure. *DFT and Multiplet and Spin−Orbit Interactions.* In the preceding discussion we have described the ground states of the $AnO_2(H_2O)_5^{2+}$ species having singlet $5f\delta^0$, doublet $5f\delta^1$, and triplet $5f\delta^2$ configurations, respectively, as shown in Figure 2. These states would be anticipated by occupation of the lowest virtual orbital and maintaining high spin coupling according to Hund's rule. While the $D_{\infty h}$ symmetry (d, f, etc.) used to denote these 5f orbitals according to the AnO_2^{2+} parent species is no longer preserved in the complex, the DFT results correspond closely to this picture as found in the occupations of the $5f\delta$ atomic orbitals.

TABLE 7: Results of Model CI and Spin−Orbit CI Calculations PuO_2^{+3}, PuO_2^{+2}, and PuO_2^{+1}

state	relative energy (eV) without spin−orbit	state (Ω) (major component)	relative energy (eV) with spin−orbit
	$PuO_2(H_2O)_5^{+3}$ f^1 states		
$^2\Delta$ (δ^1)	0.0	5/2	−0.40
		3/2	−0.38
$^2\Phi$ (ϕ^1)	0.96	7/2	+0.46
		5/2	+0.51
$^2\Pi$ (π^1)	2.80	1/2	+2.65
		3/2	+3.03
	$PuO_2(H_2O)_5^{+2}$ f^2 states		
^3H ($\delta^1\,\phi^1$)	0.0	4 (^3H)	−0.84
$^3\Sigma^-$ (δ^2, ϕ^2)	0.22	0 ($^3\Sigma^-$)	0.49
$^3\Pi$ ($\delta^1\,\phi^1$)	0.80	5 (^3H)	0.82
$^1\Gamma$ (δ^2)	1.12	1 ($^3\Sigma^-$)	0.87
$^1\Sigma^+$ (δ^2, ϕ^2)	1.14	0 ($^3\Pi$)	1.05
^1H ($\delta^1\,\phi^1$)	1.49	0 ($^3\Pi$)	1.49
1Π ($\delta^1\,\phi^1$)	2.75	6 (^3H)	1.62
$^3\Pi$ ($\delta^1\,\phi^1$)	2.79	2 ($^3\Pi$)	1.80
		1 ($^3\Pi$)	1.83
		4 ($^1\Gamma$)	2.04
		5 (^1H)	2.36
		0 ($^3\Pi$)	2.99
$^3\Sigma^-$ (δ^2) SCF	[0.78]		
	$PuO_2(H_2O)_5^{+1}$ f^3 states		
^4I ($\delta^1\,\phi^1\,\pi^1$)	0.0	15/2 (^4I)	−0.93
$^4\Phi$ ($\delta^2\,\phi^1$)	0.60	9/2 ($^4\Phi$)	+0.29
$^2\Delta$($\delta^2\,\phi^1$)	0.73		
$^4\Phi$($\delta^2\,\phi^1$) SCF	[0.90]		

For states with 2 or more unpaired electrons, the issue of treating multiplet effects in DFT[41−48] remains an area of active investigation in DFT theory. Similarly, approaches for describing excited states of molecules are also being developed within time-dependent DFT frameworks,[49−54] but most methods to date start with a closed shell ground state which is not an appropriate starting point for actinide complexes. Multiplet effects must be considered for the ground as well as excited states in molecules where these strong two-electron interactions and where single reference configurations may not adequately describe the electronic states in question. This situation arises in many atomic states, in $3d^n$ configurations of transition metal complexes, and in $4f^n$ and $5f^n$ configurations of lanthanide and actinide compounds. We will also point out where results of single-configuration DFT calculations do not agree with experimental assignments for the ground electronic state.

To examine this issue more closely, we carried out small CI calculations on a model series of compounds PuO_2^{3+} (f^1), PuO_2^{2+} (f^2), and PuO_2^{+} (f^3) in order to gain some understanding of the multiplet effects, which should be transferable to a large degree to the aquo complexes since we are assuming a "weak ligand field" model for these complexes. In addition spin−orbit effects are also included in an approximate treatment of the PuO_2^{q+} series. These results, which are summarized in Table 7 and in Figures 7−9, will be discussed below. All of the present results were obtained for $R_{Pu-O} = 1.75$ Å corresponding to a typical bond length in an actinyl complex, which is somewhat longer than would be obtained for an isolated triatomic actinyl ion. We will also compare these results with more accurate studies of "bare" AnO_2^{q+} carried out by multireference spin−orbit configuration calculations by other investigators. The present model studies, these previous theoretical results, and spectroscopic studies on actinyl species are all in relative agreement with one another with regard to the ground states of

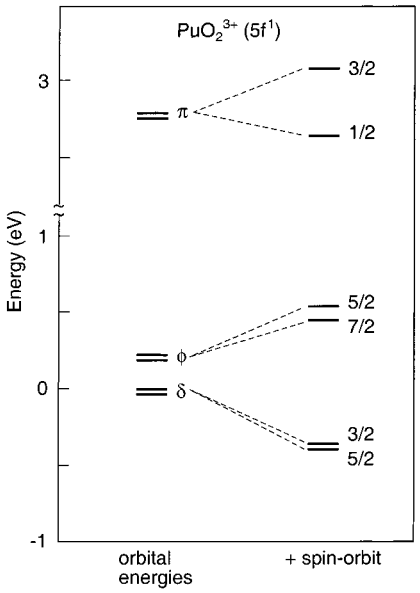

Figure 7. $5f^1$ energy levels of PuO_2^{3+} species including spin−orbit coupling.

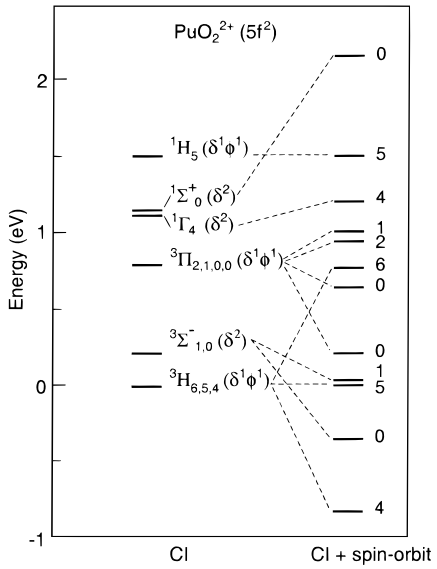

Figure 8. Low-lying states of PuO_2^{2+} including $5f^2$ multiplet interactions and spin−orbit coupling.

actinyl aquo complexes with f^2 and f^3 configurations, but they differ from the results of single configuration DFT calculations.

While these model calculations were carried out with Hartree−Fock orbitals as the starting point, one could also carry out a similar calculation including multiplet effects using the DFT orbitals as the reference. These specific types of interactions that give rise to the multiplet splittings of the 5f manifold, while obtained within a conventional CI framework, would not be explicitly included in the correlation effects normally incorporated in the exchange-correlation functionals employed in DFT theory. For this reason we will add the multiplet lowerings obtained with respect to the reference SCF state to the DFT results in order to compare energies of molecules which differ in the number of unpaired 5f electrons.

PuO_2^{3+} f^1 States. We first consider the f^1 manifold in PuO_2^{3+} (and the isoelectronic UO_2^{1+} and NpO_2^{2+} species), where there are no multiplet effects, before considering the f^2 and f^3 manifolds for the lower oxidation states. At the one electron level (Figure 7) the orbital ordering δ (0.0 eV) < ϕ (0.26 eV) < π (2.80 eV) is obtained (Figure 7). As we mentioned, we are assuming a "weak ligand field" model whereby the bare actinyl is considered as a model for the hydrated species. We note in support of this model that the order of MOs of the bare plutonyl species is similar to the virtual orbitals in the hydrated $UO_2(H_2O)_5^{2+}$ species.

When spin−orbit effects are included by diagonalizing the one-electron Hamiltonian, one obtains the results shown in Figure 7 and Table 7. The δ^1 and ϕ^1 low-lying states are split into four levels with the $\Omega = {}^5/_2$ state (where $\Omega = \Lambda + S$) lying very slightly below (0.02 eV) the $\Omega = {}^3/_2$ state. We shall denote the total spin−orbit correction as the difference in energy between the δ^1 state and the lowest spin−orbit root, which is −0.40 eV for the case of PuO_2^{3+}, as shown in Table 8. The spin−orbit contribution is determined by repeating this process with the effective spin−orbit parameters for U and Np, respectively, the results of which are shown in Table 8. For NpO_2^{+} (for $R_{Np-O} = 1.61$ Å) the CI−SO calculations of Matsika and Pitzer[26] also found a near degeneracy for the two lowest states $\Omega = {}^5/_2 < \Omega = {}^3/_2$ (0.05 eV) with $\Omega = {}^5/_2$ (0.69 eV) and $\Omega = {}^7/_2$ (0.81 eV) lying at higher energies.

PuO_2^{2+} f^2 States. The DFT results on $PuO_2(H_2O)_5^{2+}$ reported in section III.3 as summarized in Table 3 are consistent with a

TABLE 8: Multiplet and Spin−Orbit Contributions to Ground State Energies Relative to the Single Configuration Obtained from DFT Calculations (All Quantities in eV)

	ΔE_{mult}	ΔE_{so}	ΔE_{tot}
$UO_2(H_2O)_5^{+2}$ f^0	0.0	0.0	0.0
$UO_2(H_2O)_5^{+}$ f^1	0.0	−0.31	−0.31
$NpO_2(H_2O)_5^{+2}$ f^1	0.0	−0.35	−0.35
$PuO_2(H_2O)_5^{+3}$ f^1	0.00	−0.40	−0.40
$NpO_2(H_2O)_5^{+}$ f^2	−0.78	−0.74	−1.52
$PuO_2(H_2O)_5^{+2}$ f^2	−0.78	−0.84	−1.62
$PuO_2(H_2O)_5^{+1}$ f^3	−0.90	−0.93	−1.83

($5f\delta^2$) ground state. Similarly one obtains results athe $^3\Sigma^-$ ($5f\delta^2$) ground state in single-configuration Hartree−Fock calculations on PuO_2^{2+} using real orbitals. The CI results for of PuO_2^{2+} are summarized in Table 7, and the lowest electronic states are shown in Figure 8. The states are labeled by the usual convention of the orbital angular momentum projection, Λ (where Σ, Π, Δ, Φ, Γ, H, and I correspond to $\Lambda = 0$, 1, ..., 6, respectively). The results show the following ordering for the lowest triplet states: ^3H ($\delta^1\phi^1$), 0.0 eV; $^3\Sigma^-$ (δ^2 and ϕ^2), 0.22 eV; and $^3\Pi$ ($\delta^1\phi^1$), 0.80 eV. At higher energies are the singlet states $^1\Gamma$ (δ^2), 1.12 eV; $^1\Sigma^+$ (δ^2 and ϕ^2); and ^1H ($\delta^1\phi^1$), 1.49 eV. The above results were also compared to a full two-electron CI in the full virtual space with very little difference between the two calculations.

Overall, the ground state obtained from the CI calculation corresponds to a $\delta^1\phi^1$ configuration with four equal determinants of equal weight involving the real $5f\phi_x$, $5f\phi_y$, $5f\delta_{x^2-y^2}$, and $5f\delta_{xy}$ orbitals. It would be represented by a single determinant in terms of complex orbitals. The self-consistent DFT single configuration, by comparison, correspond to the excited $^3\Sigma^-$ (δ^2) state. Thus, the true ground state of PuO_2^{2+} should be represented as shown in Figure 10, and similarly one would expect similar results in the aquo complex. As will be discussed below, this ground state is also in accord with other theoretical and experimental studies.

The multiplet correction for the f^2 ground state will be defined as the difference between the diagonal δ^2 matrix element, corresponding to the single configuration DFT description, and the CI ground state, corresponding to the actual $\delta^1\phi^1$ ground state. This difference (0.77 eV) is comprised of two parts: (a) the CI splitting between the ^3H (δ^1 ϕ^1) and $^3\Sigma^-$ (δ^2 and ϕ^2)

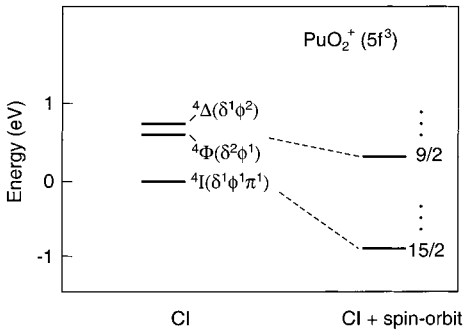

Figure 9. Low-lying states of PuO_2^{3+} including $5f^3$ multiplet interactions and spin−orbit coupling.

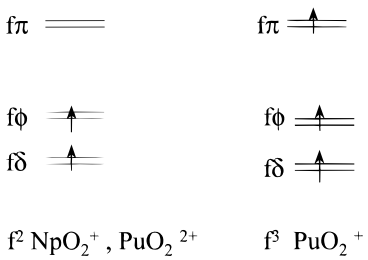

Figure 10. Schematic MO representation for the ground states of the $AnO_2(H_2O)_5^{q+}$ species including multiplet effects.

states (0.21 eV) plus the CI lowering from the diagonal d^2 element in the $^3\Sigma^-$ (δ^2 and ϕ^2) state (0.56 eV).

When spin−orbit effects are included, the lowest state is the $\Omega = 4$ state derived primarily from the ^3H ($\delta^1\,\phi^1$) state discussed above. The ^3H state with $\Lambda = 5$ also gives rise to the lowest $\Omega = 5$ and 6 states in the diagram. Overall the spin−orbit lowering in this model for the ground state is −0.84 eV.

For the PuO_2^{2+} species in matrix environments it has experimentally been determined by spectroscopic[55] and esr[56] studies that the ground state is indeed ^3H, as contrasted with the DFT δ^2 ($^3\Sigma^-$) ground state. The present results are also in quite reasonable agreement with the much more elaborate spin−orbit CI results reported recently for $5f^2$ electronic states of actinyl species recently by Maron et al.[25] on PuO_2^{2+}, by Matsika and Pitzer[26] on NpO_2^{+} and Blaudeau et al.[23] on PuO_2^{2+}. They all agree on the nature of the $\Omega = 4$ ground-state arising from the ^3H ($\delta^1\,\phi^1$) configuration and of low-lying states 0 ($^3\Sigma^-$) < 5 (^3H) < 1 ($^3\Sigma^-$) but then diverge from one another and from these results for higher states. Maron et al. reported vertical excitation energies at 1.67 Å, whereas Blaudeau et al. gave adiabatic excitation energies. Our results correspond to vertical exciations energies at 1.75 Å. The splitting between the $\Omega = 4$ and $\Omega = 1$ lowest excited state in these two previous calculations are 0.53 and 0.49 eV compared to 0.22 eV here.

PuO_2^{+} f^3 States. A similar calculation was carried out on the possible $5f^3$ states for PuO_2^{1+}. The lowest $S = {}^3/_2$ state from the CI calculations was found to be, perhaps surprisingly, the ^4I state corresponding to the $\delta^1\,\phi^1\,\pi^1$ configuration (Table 7 and Figure 9). The state corresponding to the DFT solution in Figure 2, the $^4\Phi$ state with a $\delta^2\,\phi^1$ configuration, was 0.60 eV higher in energy. While the $5f\pi$ orbital is significantly higher than the other orbitals in Figure 2 in terms of one-electron interactions, the fact that his turns out to be the lowest electronic state can be understood in terms of the two-electron interactions. For an actinide atom such as U^{3+} with a $5f^3$ configuration, the lowest L−S multiplet is the ^4I state which corresponds to the maximum orbital angular momentum ($L = 6$). The state can be represented as the determinant $f_{+3}\,{}^1f_{+2}\,{}^1f_{+1}{}^1$ which can be seen to be the same configuration in the CI ground state. The overall multiplet correction for the PuO_2^{+} ^4I ground state relative is 0.30 eV for the ^4F $\delta^2\,\phi^1$ state and 0.90 eV relative to the single reference $\delta^2\,\phi^1$ diagonal energy. When spin−orbit coupling is included, the lowest state with $\Lambda = 6$ gives a state with extremely high total angular momentum projection $\Omega = 15/2$ with a spin−orbit lowering of −0.93 eV.

TABLE 9: Vibrational and Solvent Contributions to Calculated Reduction Potentials (All Quantities in eV). Multiplet and Spin−Orbit Corrections Have Been Added in the Last Column

	E_{elec}	ΔG^{298}	ΔG^{soln}	$+\Delta E_{mul}$
$UO_2(H_2O)_5^{+2} + e^- \rightarrow UO_2(H_2O)_5^{+}$	−12.1	−12.2	−6.98	−7.29
$NpO_2(H_2O)_5^{+2} + e^- \rightarrow NpO_2(H_2O)_5^{+}$	−12.92	−13.05	−7.75	−8.92
$PuO_2(H_2O)_5^{+2} + e^- \rightarrow PuO_2(H_2O)_5^{+}$	−13.44	−13.47	−7.99	−8.20
$H_3O^+ + e^- \rightarrow {}^1/_2H_2 + H_2O$			−4.92	−4.92

D. Reduction Potentials of $An(H_2O)_5^{2+}$ in Solution. With the structures, energies and vibrational properties of $AnO_2(H_2O)_5^{2+}$ and $AnO_2(H_2O)_5^{+}$ species in the first section of this paper and the corrections to the DFT ground states from spin−orbit CI calculations from the latter section, we now proceed to consider the relative energies of the +2 and +1 species in solution as measured by the reduction potential. In Table 9 , the relative energies of the +2 and +1 species as calculated from the density functional B3LYP calculations are denoted as E_{elec}, which corresponds to the negative of the adiabatic ionization potential of each molecule. The calculated reduction potentials of $AnO_2(H_2O)_5^{1+}$ decrease monotonically in the series U (−12.1), Np (−12.9), and Pu (−13.4) eV. When zero-point and thermal corrections are applied to obtain free energies at 298 K, little change is apparent in these quantities.

The solvent corrections preferentially stabilize the doubly charged actinyl species relative to the singly charged ones, as expected from a simple Born cavity model in which the stabilization is proportional to q^2. As a result, there is a net decrease by about 5 eV in the absolute magnitudes of the reduction potentials in solution ΔG_{soln} but the relative order remains unchanged (Table 9). Finally, the multiplet and spin−orbit effects associated with the unpaired electrons that are not accounted for by DFT theory are added to the final solution results. For example, for the UO_2^{2+}/UO_2^{+} couple, there is a net stabilization of −0.31 eV for UO_2^{1+} and no stabilization for UO_2^{2+}, and as a result, the half-reaction is −7.3 eV exothermic compared to −7.0 eV without the corrections.

To compare with electrochemical reduction potentials, the energy of the hydrogen ion reduction according to the half-reaction

$$H_3O^+ + e^- \rightarrow {}^1/_2\,H_2 + H_2O \qquad (6)$$

is also given as calculated in the gas phase using DFT and in solution with the same procedure. The calculated reduction potential is −4.9 eV at the same level of calculation as used for the actinyl species.

Taking the difference of the two half-reactions we obtain the overall free energy of the redox process

$$UO_2(H_2O)_5^{+2} + {}^1/_2H_2 + H_2O \rightarrow UO_2(H_2O)_5^{+1} + H_3O^+ \qquad (7)$$

in solution. As written this way, this reaction is exoergic with $\Delta G = -2.37$ eV, for the UO_2^{2+}/UO_2^{1+} system. By the definition

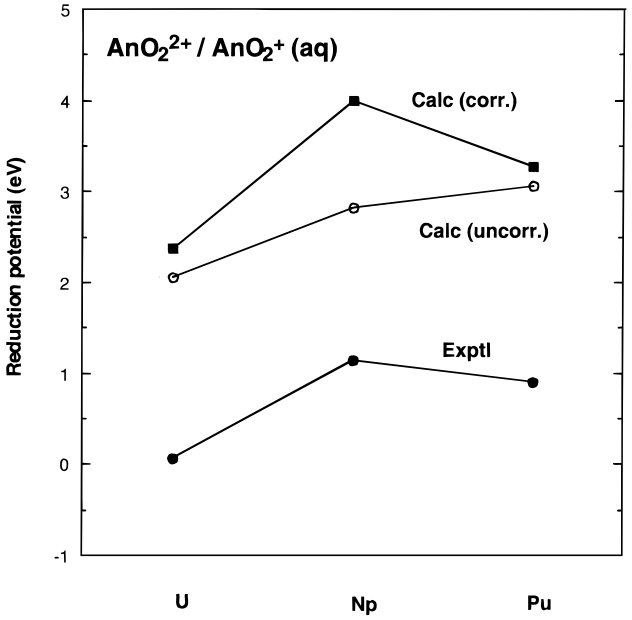

Figure 11. Comparison of experimental reduction potentials for $AnO_2(H_2O)_5^{2+}/AnO_2(H_2O)_5^{+}$ with calculated results from DFT calculations and results with multiplet and spin−orbit corrections.

TABLE 10: Comparison of Calculated and Experimental Reduction Potentials (All Quanitites in eV) Relative to the Standard Hydrogen Potential

	E^0_{calc}	E^0_{expt}
$UO_2(H_2O)_5^{+2}/UO_2(H_2O)_5^{+}$	+2.37	+0.063[a] (+0.163)[b]
$NpO_2(H_2O)_5^{+2}/NpO_2(H_2O)_5^{+}$	+4.00	+1.137[a] (+1.236)[b]
$PuO_2(H_2O)_5^{+2}/PuO_2(H_2O)_5^{+}$	+3.28	+0.913[a] (+1.013)[b]

[a] Reference 57. [b] Reference 58.

of the electrochemical potential, E^0 as the negative of the free energy,

$$\Delta G = -nFE^0 \tag{8}$$

we obtain the reduction potentials in Table 10, where they are also compared with the experimental potentials.[57,58] By this definition, all of the $AnO_2^{2+/1+}$ couples are positive relative to the hydrogen standard, i.e., the AnO_2^{2+} species are stronger oxidants than hydrogen, and the reaction as written above will proceed as written. While this is in accord with the experimental values, the *absolute* calculated values, however, are uniformly ~ 2−3 eV too high compared to experiment. Experimentally the reduction potentials in eV are U (+0.06), Np (+1.14), and Pu (+0.91), while we obtain U (+2.37), Np (+4.00), and Pu (+3.28). We shall return to this point shortly. The reduction potentials, normalized to $UO_2^{2+/1+}$ reproduce the relative trends in reduction potentials Np > Pu > U within a few tenths of an eV (Figure 11). This trend would not have been obtained simply by taking the SCF results from the DFT calculations with solvent corrections. Only when the multiplet corrections have been included do we obtain the proper trend in reduction potentials as one proceeds from U to Np to Pu.

The systematic 2−3 eV error overall is more troublesome to analyze. This could arise from various effects: (1) the dielectric continuum model, (2) the B3LYP density functional, or (3) the effective potential used in the calculations. While the dielectric continuum model is relatively simple, we have had good experience in predicting free energies of organic neutral and ionic species in solution using standard atomic radii without readjustments. Similarly excellent agreement with experiment (within 1−3 kcal/mol) was obtained for Fe(III) hydrolysis reactions using this approach.[34]

TABLE 11: Comparison of Calculated Ionization Potentials of $UO_2(H_2O)_5^{+1}$ Using Various DFT Methods and ECPs

method	HF ECP	LDA ECP	all-electronic ADF
vertical IP (eV)[a]			
LDA	10.05	9.25	9.13
BLYP	11.47		10.76
B3LYP	11.34	10.44	
adiabatic IP (eV)[b]			
B3LYP	12.07		

[a] Results at LDA geometry of $UO_2(H_2O)_5^{+2}$. [b] Results at respective geometries of +2 and +1 species.

To address the dependence on functionals and ECPs, the vertical gas-phase IP of $UO_2(H_2O)_5^{+1}$ was calculated using various methods. The LDA geometry, which is closest to the solution EXAFS results, is used for both the +1 and +2 species. The results are summarized in Table 11. LDA (SVWN5), BLYP, and B3LYP calculations were carried out using the present (HF-based) ECP for U. These IPs vary from 10.0 to 11.5 to 11.3 eV for these respective levels of DFT methods. These results were also compared to all-electron, frozen core LDA and BLYP calculations using the ADF code. In both cases the ECP results tend to overestimate the IP by about 0.7−0.8 eV compared to the ADF results. Ignoring such differences between the calculations as the use of Slater basis functions for ADF and Gaussian basis functions here, this would indicate a possible overestimate if the IP by the use of the Hartree−Fock-based ECP for B3LYP calculations.

This conclusion is supported by other calculations involving two different ECPs. The first case employed an ECP based on a relativistic LDA atomic calculation[59] with the same number of core electrons (78). This calculation gives essentially the same I.P (within 0.1 eV) as the ADF all-electron LDA calculation, as shown in Table 11. A second case employed the pseudopotential or ECP developed by Kuchel et al.[60] on the basis of a scalar relativistic HF atomic calculation with fewer electrons (60) in the core. The calculatied IP from a B3LYP calculation with this ECP (9.27 eV) is about 2 eV lower than the comparable result in Table 11 (11.34 eV) with the "larger core" ECP used throughout this paper. Assuming this difference carries over to the Np and Pu species, this would bring the absolute calculated and experimental redox potentials (Figure 11) into close agreement.

At this point we are unable to assess the hybrid functional with either an all-electron calculation or ECP based on a hybrid atomic calculation. Overall it appears that absolute ionization potentials can vary by 1−2 eV due to the choice of ECP and as much as 1.5 eV in the choice of functional. Relative IPs as a function of metal or ligand appear to be much less sensitive to these choices, but further work on more systematic comparisons is clearly warranted.

Conclusions

The structures and vibrational frequencies of $AnO_2(H_2O)_5^{2+}$ and $AnO_2(H_2O)_5^{+}$ species have been calculated using density functional theory (DFT) and relativistic effective core potentials (RECPs). The resulting structures are compared to EXAFS solution studies, where good agreement is found for the An = O bond lengths while the An-OH_2 bond lengths are typically overestimated by 0.07−0.10 Å. The calculated Raman and IR vibrational frequencies of the actinyl unit decrease in the order

U > Np > Pu for both An(VI) and An(V) oxidation states. The fact that the actinyl bond lengths are getting slightly shorter while the bond strengths are decreasing, according to the calculated frequencies, is attributed to the decreased overlap between the oxygen orbitals and the actinide 5f orbitals, which are getting progressively smaller as atomic number increases.

Free energies for reactions in solution are computed by combining thermodynamic free energies in the gas phase with a dielectric continuum model to treat solvent effects. Using this approach the hydrolysis reaction of $UO_2(H_2O)_5^{2+}$ to form $UO_2(H_2O)_4(OH)^{+}$ and the reactions for removing or adding a water to the first shell in $UO_2(H_2O)_5^{+2}$ are examined. While the five-coordinate structure is not favored either from the electronic energies or from gas-phase free energies, when solvent effects are included it becomes the most stable species.

Overall DFT provides a good description of the ground-state structure and chemical properties as long as the oxidation state remains unchanged. When the details of $5f^2$ and $5f^3$ multiplets become important, as in electronic spectroscopy or in redox properties, multiplet and spin−orbit effects should be included. Modest spin−orbit CI (SO−CI) calculations on PuO_2^{q+} as a "weak ligand field" model for the aquo complexes are presented. The DFT results gave a $(5f\delta)^2$ ground-state configuration for $NpO_2(H_2O)_5^{2+}$ and a $(5f\delta)^2$ $(5f\phi)^1$ configuration for $PuO_2(H_2O)_5^{2+}$, but in the SO−CI calculations the respective ground states are found to be $(5f\delta)^1$ $(5f\phi)^1$ for Np(VI) and $(5f\delta)^1$ $(5f\phi)^1$ $(5f\pi)^1$ for Pu(VI) using this model. These results for $5f^2$ multiplets are also in agreement with more sophisticated SO−CI calculations on AnO_2^{q+} species. The reduction potentials for all three $AnO_2(H_2O)_5^{2+}$ complexes in solution are compared with electrochemical experimental data. The correct overall trend Np > Pu > U is found when multiplet and spin−orbit corrections are included, although the absolute reduction potentials are overestimated in all three cases. The possible reasons for this overestimate are examined by comparing results using various functionals, different effective core potentials, as well as all-electron results using the ADF method.

Acknowledgment. This work was supported under Laboratory Directed Research and Development funding at Los Alamos under the auspices of the U.S. Department of Energy (Grant W-7405-ENG-36) and also from support by the Seaborg Institute for Transactinium Science at Los Alamos. The authors acknowledge C.D. Tait, D. W. Keogh, D. E. Morris, M. P. Neu, and D. L. Clark for helpful discussions and for providing experimental data prior to publication.

References and Notes

(1) Katz, J. J.; Seaborg, G. T.; Morss, L. R. *The Chemistry of the Actinide Elements*, 2nd ed.; Chapman and Hall: New York, 1986.
(2) Clark, D. L.; Hobart, D. E.; Neu, M. P. *Chem. Rev.* **1995**, *95*, 25.
(3) Pepper, M.; Bursten, B. E. *Chem. Rev.* **1991**, *91*, 719.
(4) Baerends, E. J.; Gritsenko, O. V. *J. Phys. Chem. A* **1997**, *101*, 5383.
(5) Schreckenbach, G.; Hay, P. J.; Martin, R. L. *J. Comput. Chem.* **1999**, *20*, 70−90.
(6) Hay, P. J.; Martin, R. L. *J. Chem. Phys.* **1998**, *109*, 3875.
(7) Schreckenbach, G.; Hay, P. J.; Martin, R. L. *Inorg. Chem.* **1998**, *37*, 4442−4451.
(8) Combes, J.-M.; Chisholm-Brause, C. J.; Brown Jr., G. E.; Parks, G. A.; Conradson, S. D.; Eller, P. G.; Triay, I. R.; Hobart, D. E.; Meijer, A. *Environ. Sci. Technol.* **1992**, *26*, 376.
(9) Allen, P. G.; Bucher, J. J.; Shuh, D. K.; Edelstein, N. M.; Reich, T. *Inorg. Chem.* **1997**, *36*, 4676.
(10) Conradson, S. D. *Appl. Spectrosc.* **1998**, *52*, 252A.
(11) Wahlgren, U.; Moll, H.; Grenthe, I.; Schimmelpfennig, B.; Maron, L.; Vallet, V.; Gropen, O. *J. Phys. Chem. A* **1999**, *103*, 8257.
(12) Tait, C. D. Presented at the Symposium on Heavy Element Complexes: The Convergence of Theory and Experiment, 217th ACS National Meeting, 1999, Anaheim, CA.
(13) Clark, D. L. Presented at the Symposium on Heavy Element Complexes: The Convergence of Theory and Experiment, 217th ACS National Meeting, 1999, Anaheim, CA.
(14) Aberg, M.; Ferri, D.; Glaser, J.; Grenthe, I. *Inorg. Chem.* **1983**, *22*, 3986.
(15) Basile, L. J.; Sullivan, J. C.; Ferraro, J. R.; LaBonville, P. *Appl. Spectrosc.* **1974**, *28*, 142.
(16) Toth, L. M.; Begun, G. M. *J. Phys. Chem.* **1981**, *85*, 547.
(17) Madic, C.; Begun, G. M.; Hobart, D. E.; Hahn, R. L. *Inorg. Chem.* **1984**, *23*, 1914.
(18) Guillaume, B.; Begun, G. M.; Hahn, R. L. *Inorg. Chem.* **1982**, *21*, 1159.
(19) Jones, L. H.; Penneman, R. A. *J. Chem. Phys.* **1953**, *21*, 542.
(20) Spencer, S.; Gagliardi, L.; Handy, N. C.; Ioannou, G. G.; Skylaris, C. K.; Simper, W. A. *J. Phys. Chem. A* **1999**, *103*, 1831.
(21) Tsushima, S.; Suzuki, A. *J. Mol. Struct. (THEOCHEM)* **1999**, *487*, 33.
(22) Craw, J. S.; Vincent, M. A.; Hillier, I. H.; Wallwork, A. L. *J. Phys. Chem.* **1995**, *99*, 10181.
(23) Blaudeau, J.-P.; Bursten, B. E.; Pitzer, R. M. Presented at the Symposium on Heavy Element Complexes: The Convergence of Theory and Experiment, 217th ACS National Meeting, 1999, Anaheim, CA.
(24) Ismail, N.; Heully, J.-L.; Saue, T.; Daudey, J.-P.; Marsden, C. J. *Chem. Phys. Lett.* **1999**, *300*, 296.
(25) Maron, M.; Leininger, T.; Schimmelpfennig, B.; Vallet, V.; Heully, J.-L.; Teicthteil, C.; Gropen, O.; Wahlgren, U. *Chem. Phys.* **1999**, *244*, 195.
(26) Matsika, S.; Pitzer, R. M. 1999. Unpublished.
(27) Zhang, Z. Y.; Pitzer, R. M. *J. Phys. Chem. A* **1999**, *103*, 6830.
(28) Becke, A. D. *J. Chem. Phys.* **1993**, *98*, 5648.
(29) Lee, C.; Yang, W.; Parr, R. G. *Phys. Rev. B* **1988**, *37*, 785.
(30) Vosko, S. H.; Wilk, L.; Nusair, M. *Can. J. Chem.* **1980**, *58*, 1200.
(31) Becke, A. *Phys. Rev. A* **1988**, *37*, 3098.
(32) Frisch, M. J.; Trucks, G. W.; Schlegel, H. B.; Gill, P. M. W.; Johnson, B. G.; Robb, M. A.; Cheeseman, J. R.; Keith, T.; Petersson, G. A.; Montgomery, J. A.; Raghavachari, K.; Al-Laham, M. A.; Zakrzewski, V. G.; Ortiz, J. V.; Foresman, J. B.; Cioslowski, J.; Stefanov, B. B.; Nanayakkara, A.; Challacombe, M.; Peng, C. Y.; Ayala, P. Y.; Chen, W.; Wong, M. W.; Andres, J. L.; Replogle, E. S.; Gomperts, R.; Martin, R. L.; Fox, D. J.; Binkley, J. S.; Defrees, D. J.; Baker, J.; Stewart, J. P.; Head-Gordon, M.; Gonzalez, C.; Pople, J. A. *Gaussian 98*, Revision A.7; Gaussian, Inc.: Pittsburgh, PA, 1995.
(33) Hummer, G.; Pratt, L. R.; Garcia, A. E. *J. Phys. Chem. A* **1998**, *98*, 102.
(34) Martin, R. L.; Pratt, L. R.; Hay, P. J. *J. Phys. Chem. A* **1998**, *102*, 3565.
(35) Martin, R. L.; Saxe, P. W.; Lengsfield, B. H., III; Page, M. MESA: Los Alamos, NM.
(36) Baerends, E. J.; Bérces, A.; Bo, C.; Boerrigter, P. M.; Cavallo, L.; Deng, L.; Dickson, R. M.; Ellis, D. E.; Fan, L.; Fischer, T. H.; Fonseca Guerra, C.; van Gisbergen, S. J. A.; Groeneveld, J. A.; Gritsenko, O. V.; Harris, F. E.; van den Hoek, P.; Jacobsen, H.; van Kessel, G.; Koostra, F.; van Lenthe, E.; Osinga, V. P.; Philipsen, P. H. T.; Post, D.; Pye, C. C.; Ravenek, W.; Ros, P.; Schipper, P. R. T.; Schreckenbach, G.; Snijders, J. G.; Sola, M.; Swerhone, D.; te Velde, G.; Vernooijs, P.; Versluis, L.; Visser, O.; van Wezenbeek, E.; Wiesenekker, G.; Wolff, S. K.; Woo, T. K.; Ziegler, T. ADF 1999; Theoretical Chemistry, Vrije Universiteit: Amsterdam, The Netherlands, 1999.
(37) Fonseca Guerra, C.; Snijders, J. G.; te Velde, G.; Baerends, E. J. *Theor. Chem. Acc.* **1998**, *99*, 391−403.
(38) Grenthe, I.; Fuger, J.; Konigs, R. J. M.; Lemire, R. J.; Muller, A. B.; Nguyen-Trung, C.; Wanner, H. *Chemical Thermodynamics of Uranium*; Elsevier Science Publishing Company, Inc.: New York, 1992; Vol. 1.
(39) Bardin, N.; Rubini, P.; Madic, C. *Radiochim. Acta* **1998**, *83*, 189.
(40) Rempe, S.; Pratt, L. R.; Martin, R. L.; Kress, J. K.; Redondo, A. *J. Am. Chem. Soc.* **2000**, *122*, 966.
(41) Filatov, M.; Shaik, S. *J. Chem. Phys.* **1999**, *110*, 116−125.
(42) Gilardoni, F.; Weber, J.; Hauser, A.; Daul, C. *J. Chem. Phys.* **1998**, *109*, 1425−1434.
(43) Nagy, A. *Phys. Rev. A* **1998**, *57*, 1672−1677.
(44) Yamagami, H.; Mavromaras, A.; Kubler, J. *J. Phys.-Cond. Mater.* **1997**, *9*, 10881−10900.
(45) Worthington, S. E.; Cramer, C. J. *J. Phys. Org. Chem.* **1997**, *10*, 755−767.
(46) Stuckl, A. C.; Daul, C. A.; Gudel, H. U. *J. Chem. Phys.* **1997**, *107*, 4606−4617.
(47) Petersilka, M.; Gross, E. K. U. *Int. J. Quantum Chem.* **1996**, *60*, 181−189.
(48) Becke, A. D.; Savin, A.; Stoll, H. *Theot. Chem. Acta* **1995**, *91*, 147−156.
(49) Casida, M. E. *J. Chem. Phys.* **1998**, *108*, 4439.
(50) Jomorski, C.; Casida, M. E.; Salahub, D. R. *J. Chem. Phys.* **1996**, *104*, 5134.

(51) Stratmann, R. E.; Scuseria, G. E.; Frisch, M. J. *J. Chem. Phys.* **1998**, *109*, 8218.
(52) Petersilka, M.; Grossmann, U. J.; Gross, E. K. U. *Phys. Rev. Lett.* **1996**, *76*, 1212.
(53) Bauernschmitt, R.; Ahlrichs, R.; Hennrich, F. H.; Kappes, M. M. *J. Am. Chem. Soc.* **1998**, *120*, 5052.
(54) Rosa, A.; Baerends, E. J.; vanGisbergen, S. J. A.; vanLenthe, E.; Gooeneveld, J. A.; Snijders, J. G. *J. Am. Chem. Soc.* **1999**, *121*, 10356.
(55) Denning, R. G. *Struct. Bonding* **1992**, *50*, 121.
(56) Bleany, B. *Discuss. Faraday Soc.* **1955**, *19*, 112.
(57) Bard, A. J., Ed. *Encyclopedia of Electrochemisty of the Elements*; M. Dekker: New York, 1973; Vol. 8.
(58) Brand, J. R.; Cobble, J. W. *Inorg. Chem.* **1970**, *9*, 912.
(59) Hay, P. J. Unpublished.
(60) Kuchle, W.; Dolg, M.; Stoll, H.; Preuss, H. *J. Chem. Phys.* **1994**, *100*, 7535.
(61) Alcock, N. W.; Esperas, S. *J. Chem. Soc., Dalton Trans.* **1977**, 893.